

Supporting Information

NaCo₂(SeO₃)₂(OH): Competing Magnetic Ground States of a New Sawtooth Structure with 3d⁷ Co²⁺ Ions

Liurukara D. Sanjeeva,^{a,b*} V. Ovidiu Garlea,^c Keith M. Taddei,^c Li Yin,^d Jie Xing,^d Randy S. Fishman,^d David S. Parker,^d Athena S. Sefat^d

^aUniversity of Missouri Research Reactor (MURR), Columbia, Missouri 65211, USA

^bDepartment of Chemistry, University of Missouri, Columbia, Missouri 65211, USA

^cNeutron Scattering Division, Oak Ridge National Laboratory, Oak Ridge, TN 37831, USA

^dMaterials Science and Technology Division, Oak Ridge National Laboratory, Oak Ridge, TN 37831, USA

Table SI1. Crystallographic data of NaCo₂(SeO₃)₂(OH). Parameters determined from Rietveld refinements performed using NPD collected on the HB2A diffractometer at $\lambda = 1.54 \text{ \AA}$.

Figure SI1. Hydrothermally grown single crystals of NaCo₂(SeO₃)₂(OH).

Figure SI2. Powder X-ray diffraction pattern of the ground single crystals of NaCo₂(SeO₃)₂(OH).

Figure SI3. The zigzag arrangement of the Co-Co-Co sawtooth chains on the ab-plane of the NaCo₂(SeO₃)₂(OH) structure.

Figure SI4: Magnetic spins arrangement of the individual sawtooth chain according to the proposed magnetic models for the two magnetic transitions at 11 K (T₁) and 6 K (T₂).

Figure SI5. Inelastic neutron scattering data obtained with incident energy $E_i = 25 \text{ meV}$ at two temperatures (a) 1.5 K and (c) 50 K. (c) $|\mathbf{Q}|$ -integrated cuts ($|\mathbf{Q}| = [1 - 2.5] \text{ \AA}^{-1}$) of inelastic scattering showing the presence of two bands of crystal field excitations. Vertical blue lines in (c) indicate the instrumental energy resolution (full width at half-maximum).

Figure SI6. (a) Spin-wave excitation spectrum of measured at 1.5 K using $E_i = 3.8 \text{ meV}$. (b) Inelastic spectrum measured in the partial ordered state at 8 K, ($T_1 < T < T_2$) (c) Calculated spin-wave spectrum using a simple Heisenberg Hamiltonian model that includes three intra-chain (J_{bv} , J_{bb} , J_{bv2}) and two interchain (J_{n1} , J_{n2}) exchange interactions. The magnetic exchange pathways are shown in (d).

Figure SI7. The schematic of z-directional projected ferromagnetic (FM) and antiferromagnetic (AFM) orders of Co(2) atoms NaCo₂(SeO₃)₂(OH). The yellow and blue balls corresponds to the Co(1) and Co(2) atoms, respectively.

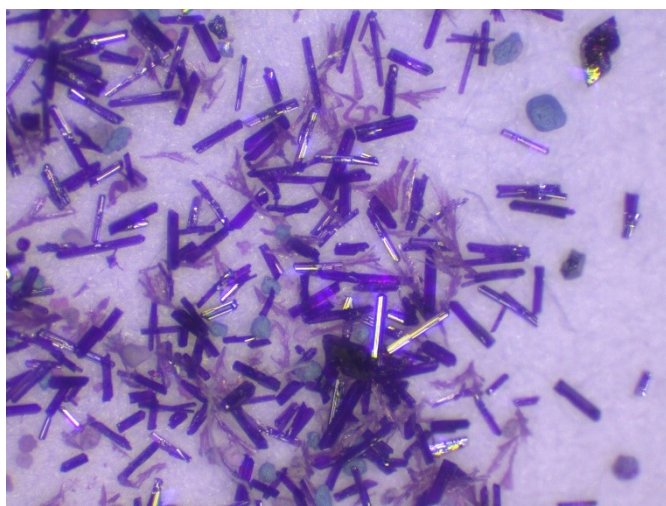


Figure SI1. Hydrothermally grown single crystals of NaCo₂(SeO₃)₂(OH).

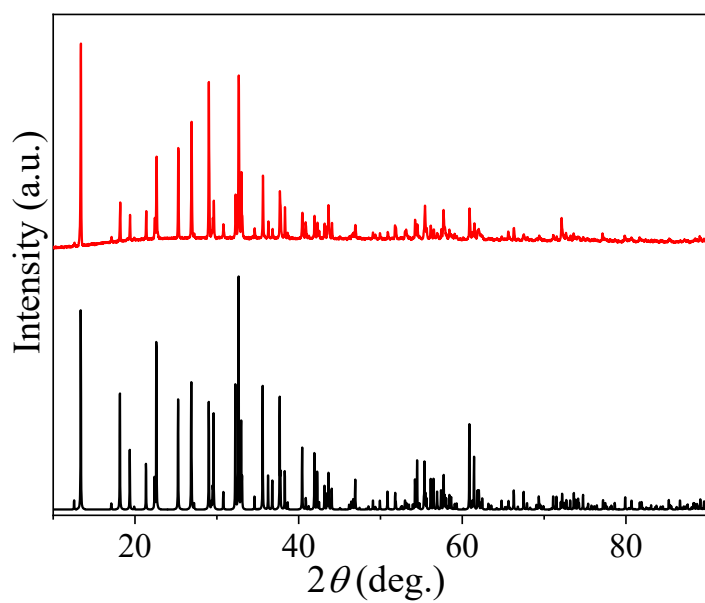


Figure SI2. A comparison of the powder X-ray diffraction pattern of the ground single crystals of NaCo₂(SeO₃)₂(OH) (red) to the calculate PXRD pattern (black) of NaCo₂(SeO₃)₂(OH) based on *Pnma* structure.

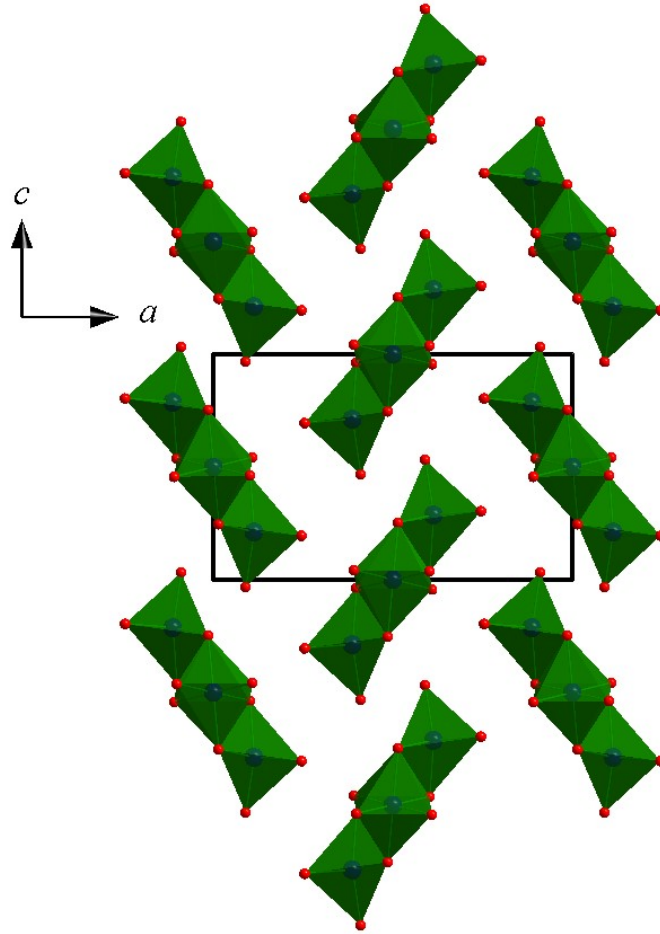


Figure S13. The zigzag arrangement of the Co-Co-Co sawtooth chains on the ab-plane of the $\text{NaCo}_2(\text{SeO}_3)_2(\text{OH})$ structure.

Table S11. Crystallographic data of $\text{NaCo}_2(\text{SeO}_3)_2(\text{OH})$. Parameters determined from Rietveld refinements performed using NPD collected on the HB2A diffractometer at $\lambda = 1.54 \text{ \AA}$.

space group, Z	<i>Pnma</i> (no.62), 4
T , K	150 K
a , \AA	13.2299(2)
b , \AA	6.02287(9)
c , \AA	8.32157(3)
volume, \AA^3	663.079(1)
R_{wp} (%)	2.26

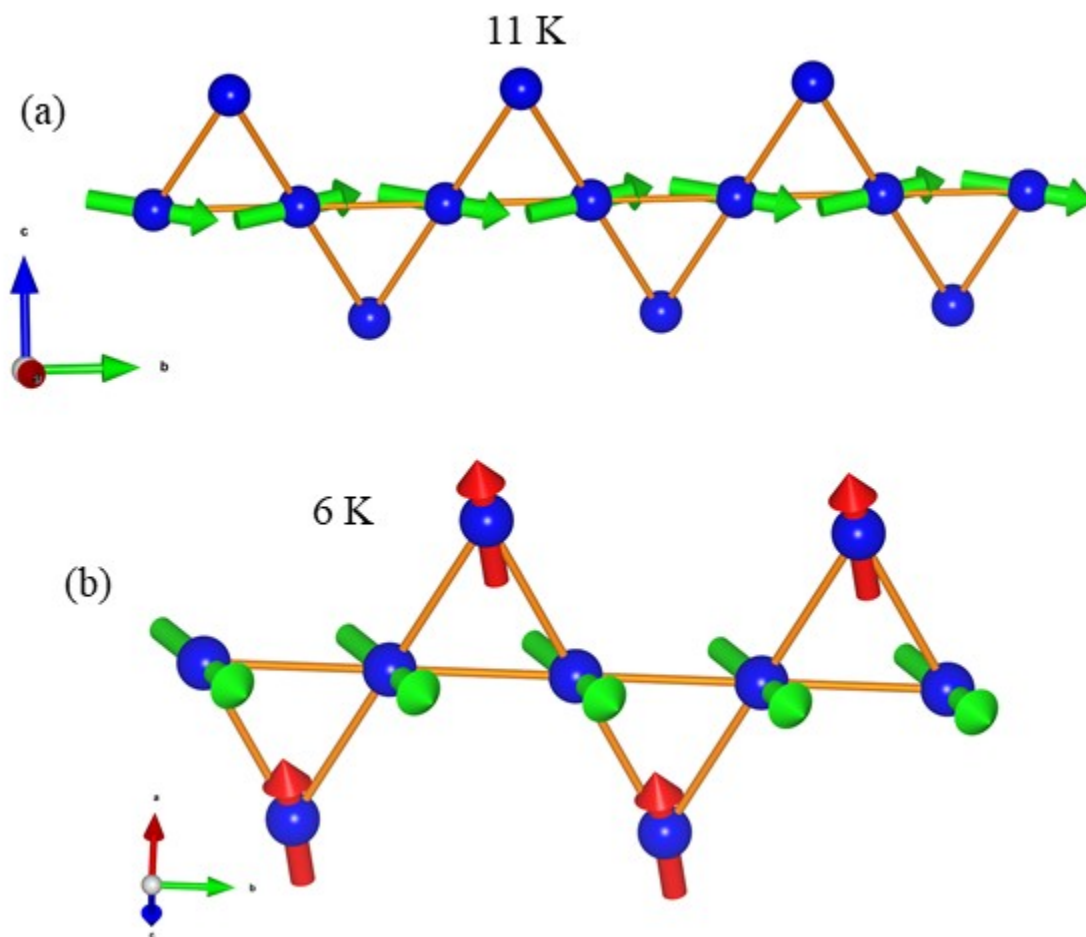


Figure S14: Magnetic spins arrangement of the individual sawtooth chain according to the proposed magnetic models for the two magnetic transitions at 11 K (T1) and 6 K (T2).

Crystal field Excitations of NaCo₂(SeO₃)₂(OH)

Neutron inelastic scattering data on polycrystalline NaCo₂(SeO₃)₂(OH) measured at 1.5 K and 50 K with an incident energy, $E_i = 25$ meV is displayed in Figure SI 4. The spectrum consists of two flat excitation bands centered at about at 7 and 17 meV, which broaden progressively as temperature increases. The $|\mathbf{Q}|$ -integrated cuts over the range 1 - 2.5 Å⁻¹, shown in Figure SI 4c, suggest that each band is structured into at least two distinct excitations *within the experimental resolution*. The instrumental energy resolution (*the full width at half maximum*) is represented by vertical blue lines in Figure SI 4c. The decay of intensity with the momentum transfer as well as the temperature dependence demonstrate the magnetic nature of the excitations. The presence of pair excitations in each band is not surprising considering the existence of two distinct Co²⁺ magnetic sites in our material.

The d^7 electrons of Co²⁺ in an octahedral crystal field can possess a multiplet state with spin $S = 3/2$ and effective orbital moment $L_{\text{eff}} = 1$. The spin-orbit coupling ($H_{\text{SO}} = \lambda \vec{L} \cdot \vec{S}$) can split this state into three states: a $J_{\text{eff}} = 1/2$ ground state, and $J_{\text{eff}} = 3/2$ and $J_{\text{eff}} = 5/2$ excited states, that are separated in energy by $3/2 \lambda$ and $5/2 \lambda$, respectively. The observation of crystal field excitations between the $J_{\text{eff}} = 1/2$ ground state and the excited states is common in cobalt compounds and provides support for the presence of the spin-orbital entangled state.¹⁻⁵ The deviation from ideal octahedral environment produces a further split of the $J_{\text{eff}} = 3/2$ and $5/2$ excited states. Moreover, the long-range magnetic order below T_N creates an internal molecular field, which induces a Zeeman splitting of the $J_{\text{eff}} = 1/2$ manifold.

The inelastic spectrum of NaCo₂(SeO₃)₂(OH) is reminiscent to the spectra observed for α -CoV₂O₆² and α, γ -CoV₃O₈⁴ that show two bands of excitations at ~ 5 meV and ~ 25 meV, which are due to transitions within the $J_{\text{eff}} = 1/2$ manifold and between the $J_{\text{eff}} = 1/2$ and $J_{\text{eff}} = 3/2$ manifolds, respectively. Similarly, we associate the flat band at 17 meV of NaCo₂(SeO₃)₂(OH) with the spin-orbit excitations between the $J_{\text{eff}} = 1/2$ and $J_{\text{eff}} = 3/2$ manifolds in the two distinct Co²⁺ sites. Furthermore, the fact that the intensity of the 7 meV excitation is significantly reduced at 50 K, above the magnetic order transition, suggests that this excitation is associated with the splitting of the lowest-energy ground-state $J_{\text{eff}} = 1/2$ doublet due to the molecular field induced by magnetic order. Hence, the observed spin-orbit excitations support the view that Co²⁺ ions of NaCo₂(SeO₃)₂(OH) have a spin-orbital entangled $J_{\text{eff}} = 1/2$ state.

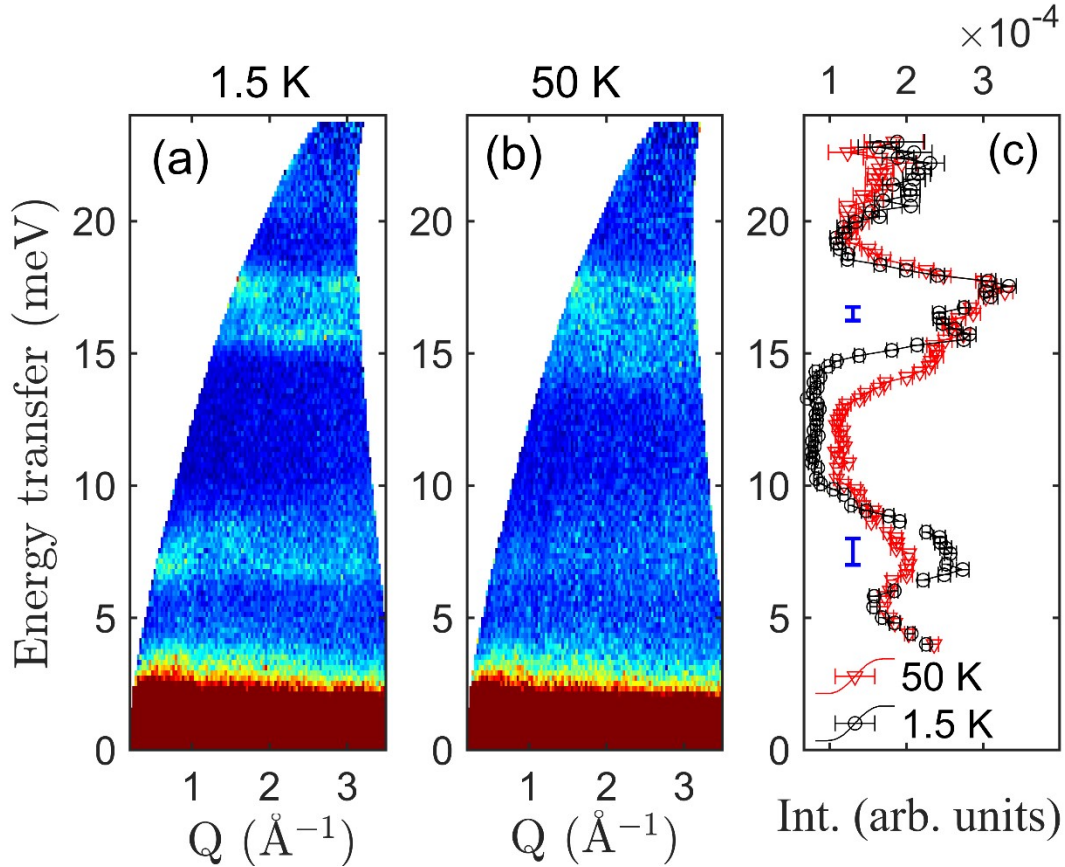


Figure SI5. Inelastic neutron scattering data obtained with incident energy $E_i = 25$ meV at two temperatures (a) 1.5 K and (c) 50 K. (c) $|\mathbf{Q}|$ -integrated cuts ($|\mathbf{Q}| = [1 - 2.5] \text{ \AA}^{-1}$) of inelastic scattering showing the presence of two bands of crystal field excitations. Vertical blue lines in (c) indicate the instrumental energy resolution (full width at half-maximum).

Spin-wave excitations of $\text{NaCo}_2(\text{SeO}_3)_2(\text{OH})$

The low-energy excitation spectrum of $\text{NaCo}_2(\text{SeO}_3)_2(\text{OH})$ was characterized using the HYSPEC spectrometer with the incident energy $E_i = 3.8$ meV. At low temperature ($T = 1.5$ K), the powdered averaged spectrum of the magnetically ordered state, shown in Figure SI 5a, features two well-defined excitation modes: one flat mode located at about 1.1 meV and a second dispersive mode that emerges at the momentum transfer $Q \approx 0.8 \text{ \AA}^{-1}$, corresponding to the $(3/2, 0, 1)$ magnetic peak, and extends up to about 0.6 meV. At 8 K, in the partially ordered state, $T_1 < T < T_2$, both excitation modes vanish, and only diffuse scattering is observed, Figure SI 5b.

An attempt of describing the spin-wave spectrum was made using a Heisenberg Hamiltonian model which includes three intrachain and two interchain exchange parameters, as depicted in Figure SI 5d. For the intrachain couplings we considered the exchange interactions between the nearest-neighbor Co(2) atoms forming the triangles base (J_{bb}), the interaction between the base

and vertex positions Co(1)–Co(2) (J_{bv}), as well as the next-nearest neighbor base-vertex interaction (J_{bv2}), Figure SI 5d. The long-range magnetic order is stabilized by additional couplings between adjacent sawtooth chains (J_{n1} and J_{n2}), that involve super-exchange pathways via [SeO₃] groups (Co(1)–O–Se–O–Co(1) or Co(1)–O–Se–O–Co(2)). The spin-wave spectrum was calculated using linear spin wave theory as implemented in the SpinW program. The analyses indicate that the main characteristics of excitation spectrum can be reproduced using the following parameters: $S \cdot J_{bb} = 0.15$ meV, $S \cdot J_{bv} = 0.4$ meV, $S \cdot J_{bv2} = 0.1$ meV, $S \cdot J_{n1} = -0.05$ meV, $S \cdot J_{n2} = -0.03$ meV. The positive J values correspond to antiferromagnetic coupling while the negative represent a ferromagnetic coupling. We found that the ferromagnet interchain couplings (J_{n1} and J_{n2}) play a key role in stabilizing the AFM order with the wavevector $\mathbf{k} = (1/2, 0, 0)$. The large ratio J_{bv}/J_{bb} could be due to the difference in Co–O–Co bond angles associated with the two exchange pathways. The Co(1)–O–Co(2) angles (J_{bv}) are $\sim 91^\circ$ and 95° , while the Co(2)–O–Co(2) (J_{bb}) angles are 97° and 100.5° . This simple Heisenberg Hamiltonian model is successful in reproducing the energy positions of two spin-wave modes but is deficient in describing the correct \mathbf{Q} dependence of the intensity for the low-energy mode (see Figure SI 5c). Moreover, the model fails in explaining the ferromagnetic components along b -direction, as well as the orthogonal arrangement between Co(1) and Co(2) moments. Considering the significant information loss in the powder averaged inelastic data, the number of parameters *that can* be tested simultaneously is drastically limited. This precludes the use of more complex models that include further neighbor interactions, biquadratic coupling or anisotropic exchange interactions that are expected to arise from the strong spin-orbit coupling in this compound. However, additional spin wave excitation studies using single crystals are needed to look for firmer quantitative evidence of intrachain and interchain exchange parameters of NaCo₂(SeO₃)₂(OH).

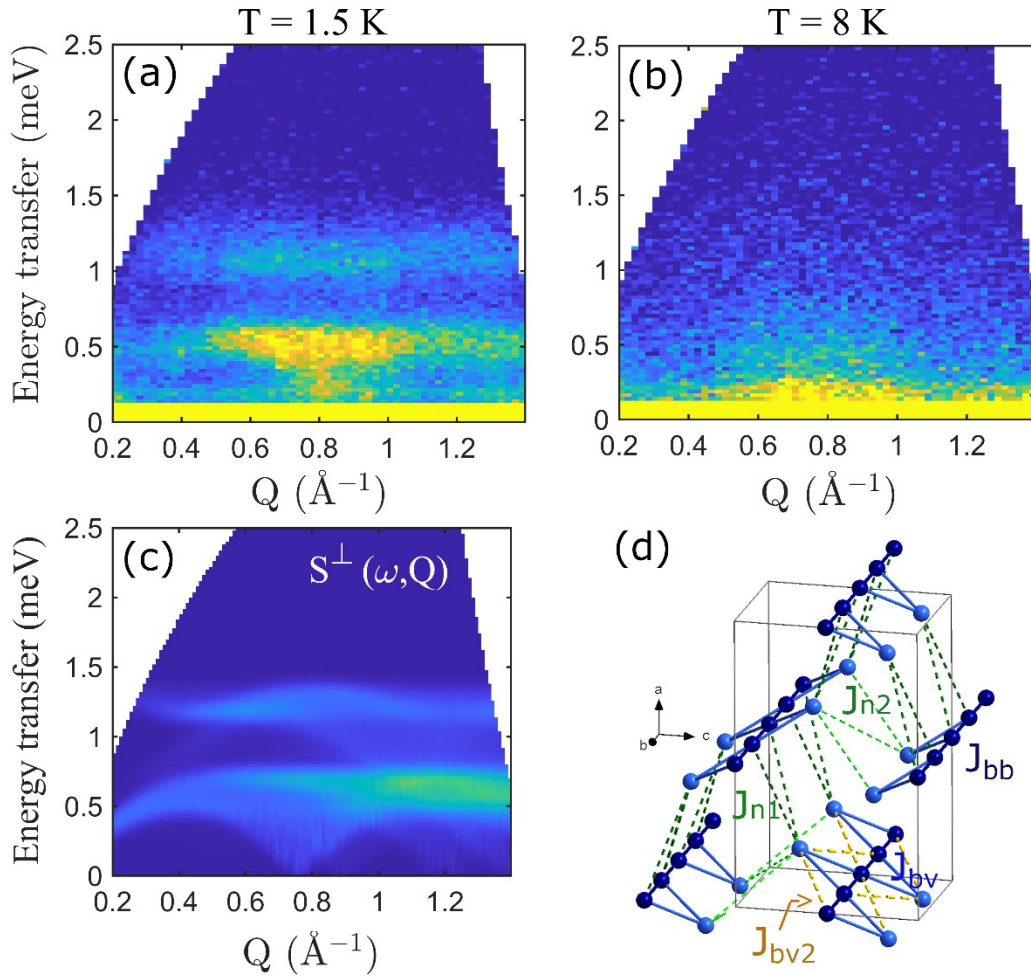


Figure SI 6. (a) Spin-wave excitation spectrum of measured at 1.5 K using $E_i = 3.8$ meV. (b) Inelastic spectrum measured in the partial ordered state at 8 K, ($T_1 < T < T_2$) (c) Calculated spin-wave spectrum using a simple Heisenberg Hamiltonian model that includes three intra-chain (J_{bv} , J_{bb} , J_{bv2}) and two interchain (J_{n1} , J_{n2}) exchange interactions. The magnetic exchange pathways are shown in (d).

- [1] Holden, T. M.; Buyers, W. J. L.; Svensson, E. C.; Cowley, R. A.; Hutchings, M. T.; Hukin, D.; Stevenson, R. W. H.; *J. Phys. C: Solid State Phys.* **1971**, *4*, 2127.
- [2] Ross, K. A.; Brown, J. M.; Cava, R. J.; Krizan, J. W.; Nagler, S. E.; Rodriguez-Rivera, J. A.; Stone, M. B. Single-Ion Properties of the $S_{\text{eff}} = \frac{1}{2}$ XY Antiferromagnetic Pyrochlores NaACo_2F_7 ($A = \text{Ca}^{2+}, \text{Sr}^{2+}$). *Phys. Rev. B* **2017**, *95*, 144414.
- [3] Wallington, F.; Arevalo-Lopez, A. M.; Taylor, J. W.; Stewart, J. R.; Garcia-Sakai, V.; Attfield, J. P.; Stock, C. Spin-orbit transitions in α - and γ - CoV_2O_6 . *Phys. Rev. B* **2015**, *92*, 125116.
- [4] Sarte, P. M.; Arévalo-López, A. M.; Songvilay, M.; Le, D.; Guidi, T.; García-Sakai, V.; Mukhopadhyay, S.; Capelli, S. C.; Ratcliff, W. D.; Hong, K. H.; McNally, G. M.; Pachoud,

- E.; Attfield, J. P.; Stock, C. Ordered Magnetism in the Intrinsically Decorated $j_{\text{eff}} = 1/2$ α - CoV_3O_8 *Phys. Rev. B* **2018**, 98, 224410.
- [5] Songvilay, M.; Robert, J.; Petit, S.; Rodriguez-Rivera, J. A.; Ratcliff, W. D.; Damay, F.; Balédent, V.; Jiménez-Ruiz, M.; Lejay, P.; Pachoud, E.; Hadj-Azzem, A.; Simonet, V.; Stock, C. Kitaev Interactions in the Co Honeycomb Antiferromagnets $\text{Na}_3\text{Co}_2\text{SbO}_6$ and $\text{Na}_2\text{Co}_2\text{TeO}_6$. *Phys. Rev. B* **2020**, 102, 224429.

First-principles calculations

First-principles calculations were performed by the density functional theory in Vienna *Ab initio* Simulation Package.¹⁻² Projector augmented wave pseudo-potentials are employed with the Perdew-Burke-Ernzerhof exchange correlation functional in the calculations.³⁻⁴ The applied energy cutoff for plane wave is 520 eV. The Brillouin Zone is sampled with Γ -centered $4 \times 9 \times 6$ k point meshes in primitive cell and $2 \times 9 \times 6$ k points in supercell with $p(2 \times 1 \times 1)$ periodicity. The calculated lattice structure of $\text{NaCo}_2(\text{SeO}_3)_2(\text{OH})$ comes from our experimental results. The convergence criteria for energy and atomic forces are 10^{-6} eV and 0.001 eV/Å, respectively. We consider the Hubbard U effect for Co $3d$ states. As shown in Figure SI6, $\text{NaCo}_2(\text{SeO}_3)_2(\text{OH})$ in ferromagnetic state is metallic in $U = 0$ or 3 eV, but insulating in $U = 5$ eV. So, we apply the $U = 5$ eV to correct the insulating characteristic of $\text{NaCo}_2(\text{SeO}_3)_2(\text{OH})$. Here, according to our experimental results, the ferromagnetic order in $\text{NaCo}_2(\text{SeO}_3)_2(\text{OH})$ is reflected only by the Co(2) and the initial magnetization of Co(1) is set to $0 \mu_B$ in our calculation. However, the finally calculated magnetic moment of $-0.92 \mu_B$ in Co(1) is antiparallel to that of $2.78 \mu_B$ in Co(2), with the U of 5 eV. The antiparallel Co(1) and Co(2) also apply to $U = 0$ and 3 eV case. These calculational results a possible antiferromagnetic orders in $\text{NaCo}_2(\text{SeO}_3)_2(\text{OH})$, which is also checked by our experimental measurements.

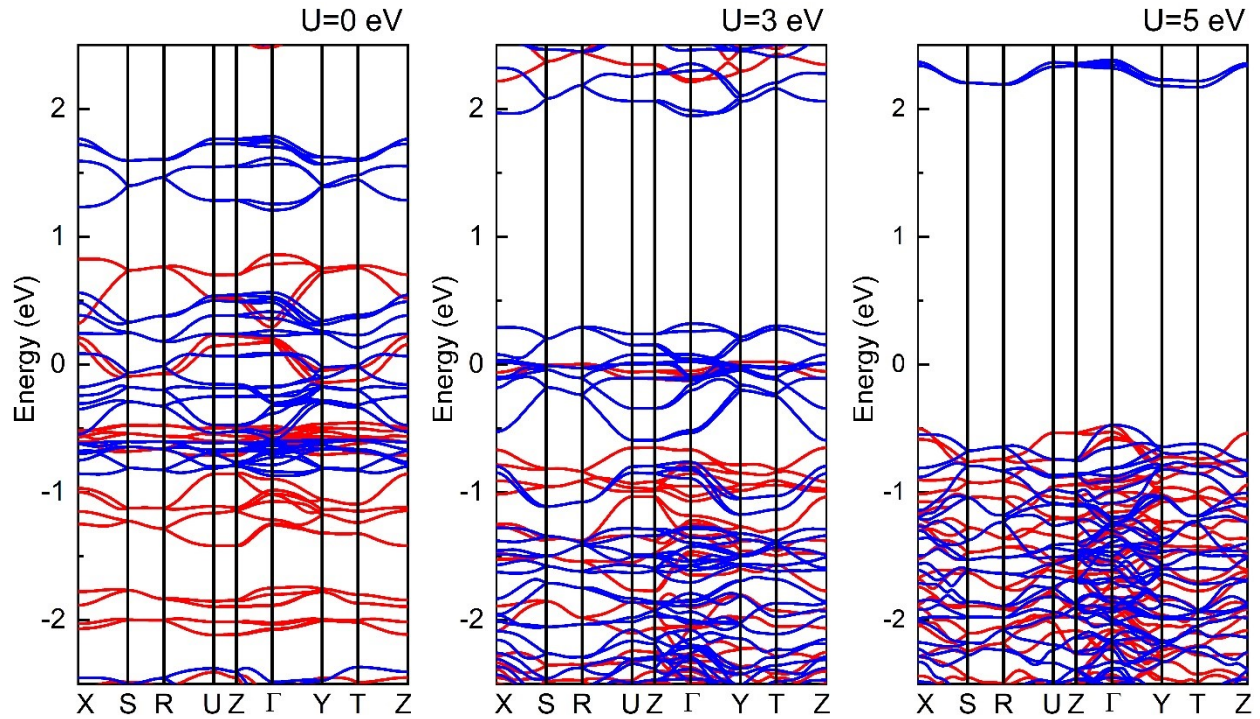


Figure SI7. The band structures of ferromagnetic $\text{NaCo}_2(\text{SeO}_3)_2(\text{OH})$ with ordered $\text{Co}(2)$ atoms under different U . The red and blue lines correspond to the spin up and down, respectively. The Fermi level is 0 eV.

- [1] Kresse, G.; Furthmüller, J. Efficiency of ab-initio Total Energy Calculations for Metals and Semiconductors Using a Plane-wave Basis Set. *Comput. Mater. Sci.* **1996**, *6*, 15–50.
- [2] Kresse, G.; Furthmüller, J. Efficient Iterative Schemes for ab-initio Total-energy Calculations Using a Plane-wave Basis Set. *Phys. Rev. B* **1996**, *54*, 11169–11186.
- [3] Blöchl, P. E. Projector Augmented-wave Method. *Phys. Rev. B* **1994**, *50*, 17953–17979.
- [4] Kresse, G. Joubert, D. From Ultrasoft Pseudopotentials to the Projector Augmented-wave Method. *Phys. Rev. B* **1999**, *59*, 1758–1775.